*Article*

# Synergistic Effects of the Urban-Rural Divide on Outdoor Airborne Bioaerosol Diffusion: A Case Study in the Monsoon Region of China

Ting Zhang [1,*], Yuying Chen [2,3], and Guiying Li [2,3]

[1] College of Civil Engineering, Liaoning Technical University, Fuxin 123000, China
[2] Guangdong-Hong Kong-Macao Joint Laboratory for Contaminants Exposure and Health, Guangdong Key Laboratory of Environmental Catalysis and Health Risk Control, Institute of Environmental Health and Pollution Control, Guangdong University of Technology, Guangzhou 510006, China
[3] Guangdong Engineering Technology Research Center for Photocatalytic Technology Integration and Equipment, Guangzhou Key Laboratory of Environmental Catalysis and Pollution Control, School of Environmental Science and Engineering, Guangdong University of Technology, Guangzhou 510006, China
* Correspondence: memchem@163.com
Received: 6 March 2024; Revised: 30 June 2024; Accepted: 20 August 2024; Published: 10 September 2024

**Abstract:** Globally, air pollution is intensifying in both urban and rural environments due to rapid urbanization and industrialization. It is widely accepted that human activities, particularly mining, contribute to increased concentrations of fine particulate matter in the atmosphere, leading to serious concerns regarding the associated health risks. In this study, the characteristics of outdoor aerosols containing bacteria and fungi were determined from on-site samples that were analyzed using sequencing techniques as well as modelling at both artificial and natural locations in two cities (Fuxin, FX; Guangzhou, GZ) in China. The interaction between urban and rural anthropogenic activities had a synergistic effect on the distribution of airborne microorganisms. At locations with artificial surfaces, which were characterized by higher population densities, the concentration of Firmicutes, including *Streptococcus pneumoniae* and *Aspergillus fumigatus*, which are colonizers of the human respiratory tract, was 1.25 times greater than that of the on-site monitored total airborne microbes (TAM) concentration. In the natural wetland area with a lower population density, the coarse-, medium-, and fine- bioaerosols accounted for 16%, 49%, and 35% of the TAM concentration, respectively. When a concentration ratio was used to describe the airborne bioaerosol (x: C/C′), the community distribution was found to vary between artificial and natural environments in FX. This was attributed to the contributions of agricultural and traffic activity. The accumulation and atmospheric diffusion of aerosols, particularly in areas with low wind speeds, led to the presence of inhalable (0.65–2.1 μm) bioaerosols. Through a modeling-based analysis, elevated x values indicated a regional deterioration in air quality due to aerosol emissions and their spatial dispersion. This ratio was highlighted by the significant abundance of Ascomycota observed at transportation infrastructure sites in GZ. The study suggests the existence of health risks associated with regional atmospheric bioaerosols, with the risks varying across the urban-rural divide.

**Keywords:** urban air quality; bioaerosol; community; atmospheric dispersion modelling; risk assessment

## 1. Introduction

The rapid industrialization of cities has worsened air quality [1,2]. More than 55% of the world's population live in urban areas subject to adverse levels of environmental pollution [3–5]. For instance, mining activities emit fine-dust capable of penetrating into the human pulmonary system, which is considered one of the biggest threats to human health and ecological environment [6]. Approximately 51% of surface mining processing areas are concentrated in five countries, namely China, Australia, the USA, Russia, and Chile, which has resulted in serious particulate matter (PM) pollution events in the atmosphere of major cities in these locations [7]. There is limited understanding of regional bioaerosol transmission. Urban airborne aerosol pollutant has caused many reported respiratory problems, such as coughs, asthma and fever. These challenges in risk prediction and control have presented obstacles in addressing public health concerns associated with air quality [8,9].

The long-range transport of dust impacts the regional climate, while during dry and wet deposition, dust can be mixed with other aerosols and airborne bacteria in the outdoor atmosphere [10]. Bioaerosols are regarded as

one of the main particulate pollutants in many urban infrastructures of China [11,12]. Dusts with diameters of 500 nm have been measured in the atmosphere of mining cities of China, and have been found to contain toxic elements [13,14]. There is a vast diversity of types, compositions, and particle size distributions of bioaerosols, and their characterization requires the mapping of the main sources, including anthropogenic activities and natural processes [15]. A rich diversity of microbial species has been identified in atmospheric dust, including potential pathogens and functional bacterial and fungal groups [16,17]. Effective air quality planning is required to control the dispersion of airborne dust in the coarse (diameter (D) > 2.5 μm) and super coarse (D >10 μm) categories [18]. However, there have been few size-fractionated bioaerosol studies in regions characterized by a strong urban-rural divide. Most studies have concentrated on size-integrated concentration metrics, such as $PM_{2.5}$, that lack essential biological particle size distribution information, and are therefore inadequate for routine air quality monitoring [19]. Rather than focusing solely on fine aerosol levels without bio-aerosol composition to explain the factors contributing to air pollution, environmental monitoring stations should provide data on detailed aerosol concentration [20]. Furthermore, the knowledge of bioaerosol diffuse concentration and component changes in diverse urban land-use areas is scarce [21].

Built-up areas account for the majority of artificial land surfaces [22], and their extent is not only an indicator of the range and intensity of human activities, but is also an important driving factor of environmental problems, such as regional climate change and environment deterioration [23]. The conversion of natural land into industrial areas can have detrimental unknown effects on the environment, involving dust pollution from mining [24,25]. The mine city outdoor environmental data of the particulates usually received contradictory inspection results and then drew more surrounding residents' attention [26]. Previous studies have predicted the spatial distribution and variability of pollutants using the geographic information system (GIS) and the inverse distance weighting method [27]. The microbial aerosol variation patterns in the air have little or no understanding in certain meteorological scenarios of these cities [28]. A validated atmospheric modelling can lead to improvements in air quality and better risk management [29,30].

Multiple linear regression, meteorological dispersion modeling, and land-use regression models are frequently used to describe the small-scale variations in outdoor air pollutant exposures [31]. Solving the Navier–Stokes equations for turbulent flows, computational fluid dynamic (CFD) models will be beneficial for environmental pollutant dispersion studies. They can also be enhanced by the input of on-site observational data [32]. An Anderson sampler can be used to rapidly detect airborne bacteria [33,34]. Besides, scientists suggested that there has been a major decline in the wind variables, which could result in regional air pollution in Asian monsoon regimes [35], possibly due to higher biological dust transports [36]. Some scientific evidence points out that the ground wind speed has weakened by up to 58% in Asia monsoon in recent decades (wind speed < 2.5 m/s), which may be caused by human factors (e.g., land use changes and air pollutant emissions) [37]. Health risks may arise from the microorganisms present in the ambient aerosol, while PM-carrying microbes from various sources have rarely been investigated in mining cities [38]. Furthermore, using data from only a few meteorological monitoring stations is not sufficient to fully assess the risks [39]. Moreover, mine dust is often incorrectly considered to be biochemically inert incorrectly [40]. Dose -response relationship modelling predicts that resource extraction activities caused airborne bio-pollutant hazards, but the exact level of risk needs to be quantified.

In this study, a practical modelling study validated by bioaerosol monitoring was conducted in two cities, with the aim of identifying the environmental effects of airborne pathogens and risks. Both the characteristics of airborne bioaerosols and inhalable PM in the air were detected various locations in Fuxin City (FX) and Guangzhou City (GZ), using on-site sampling followed by a sequencing analysis. A regional air quality modelling method was then employed using a GIS-based CFD method. A scientific modelling framework was devised for urban management on a regional scale, with a particular focus on assessing the risks associated with bioaerosols in cities rich in natural resources.

## 2. Materials and Methods

### *2.1. Sampling Location*

This study was carried out in two typical cities in China located in the Asian monsoon region. Both cities had an extensive history of mining sector and were of comparable size. The first city (FX) was located in northeast China and has a mining industry dating back to the Mao's era and is located in a temperate monsoon area (longitude and latitude: 121° E, 42° N). FX has a land area of 10,355 $km^2$ and a population of two million people (1.65 million in 2021 and 1.82 million in 2010 according to the census data). The second city (GZ) is based on light industry and is located in the subtropical monsoon region of the southeast of China (longitude and latitude: 113° E, 23° N). Approximately nineteen million people (18.68 million in 2021, 12.70 million in 2010) reside in GZ and it has a land area of 7434 $km^2$.

Within the study areas, a total of 15 sampling points (9 sampling sites in FX city and 3 sampling sites in GZ city) were chosen within the sampling areas, as shown in Figure 1 and Tables S1 and S2. Development more accurate quantification techniques to comprehend the effects of resource cities on possible environmental pollution is regarded as leading sustainability actions [41]. Therefore, in this study, there are 2 categories of urban land use division: artificial surface area ($I_{artificial}$) (built-up land for public use, involving a shopping mall, campus, parks, transportation networks, and farm land) and natural surface area ($II_{natural}$), which consisted of water resource facilities and natural wetland.

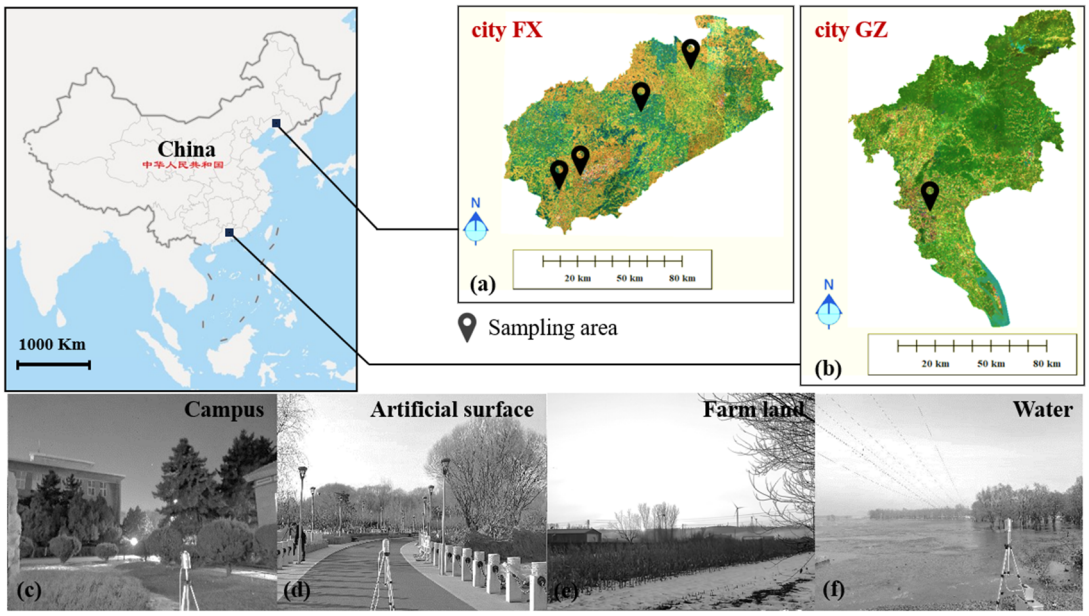


**Figure 1.** The study area in the Asian monsoon region: (**a**): FX (**b**): GZ, and (**c**–**f**): examples of sampling sites in the winter.

### *2.2. Sample Collection*

A six-stage Andersen impactor (FA-1, Weifang Aiwo Instrument Corp., Weifang, China), which can separate ambient bioaerosols in the aerodynamic diameter range of 0.65–1.1 μm to >7 μm was used to collect airborne cultivable bioaerosol samples on-site. Furthermore, an eight-stage Andersen impactor (FA-3, Aiwo Instrument Corp., Weifang, China), which has the ability to separate ambient aerosols in the aerodynamic diameter range: of 0.43– >10 μm, was also used for sampling.

During the on-site measurements, the Anderson sampling device was placed at a height of 1.5 m above the ground to collect bioaerosols from the human breathing zone. The air sampling flow rate was set to 28.3 L/min, and the sampling time was 3 min. The air volume collected for every air sample was always 0.0849 $m^3$. Before and after the sampling procedure, the flow rate of the pump was performed an advance calibration using a digital flow meter. All air samples were collected and replicated ($n$ = 2) with average values used in the analysis, and the sampler was pretreated with 75% ethanol to ensure it was disinfected.

Both a blood agar plate (BAP) and nutrient agar plate (NAP) were used to ensure accurate sampling of pathogenic particles in the air. These media allowed the ambient bioaerosol to be divided into two groups: infectious cultivable bacteria, fungi; and total cultivable bacteria, fungi. Additionally, microclimate parameters (outdoor temperature and atmospheric relative humidity, and wind speed and direction) were measured using a digital temperature and humidity, atmospheric pressure meter (DPH-102), and a digital hot-ball wind speed meter (QDF-6, Kaixingdemao Instrument Corp., Beijing, China). The on-site sampled airborne bioaerosol, involving bacterial and fungal air samples, was incubated under standard conditions: 72 h at 37 °C. Following incubation, the total cultivable bioaerosol concentration was recorded as colony numbers per agar plate (≈ 25 $cm^2$). Furthermore, the urban outdoor environmental biological community was analyzed and applied to an on-site measurement-based modelling.

In this study, water and soil samples were collected on-site from a continental slop shore site in the wetland areas. Soil sampling was carried out with a human-operated, sterile stainless-steel spoon at a depth of 5 mm below the ground surface. Each soil sample (200 ± 10 g) was placed into the sterile bags on the ice bags in a portable cold closet and moved to the laboratory for further analysis. They were stored at 5 °C, and prepared for the next

stage of analysis. All water samples (1000 ± 50 mL) were collected at least 1 m above the water surface. Water was collected with a newly developed sterile stainless-steel cup (250 mL) that allowed each sampling bowl to be completely submerged in the water body. Water was stored in 1 L sterile water sample bags. These samples were filtered through sterile membrane filters with a pore size of 0.2 μm. Each water-filtered membrane was stored in an individual sterile bag (250 mL) at −20 °C, and transported to the laboratory in an ice bag for the sequencing.

### *2.3. Amplicon Sequencing*

Amplicon sequencing is the most widely used technique for a microbiome analysis and can be applied to air, water, and soil samples. The environmental samples were subjected to DNA extraction and 16s rRNA gene amplicon sequencing (16S analysis). The 16S amplicon sequencing revealed the bacteria composition using a next-generation sequencing. Comparative studies of the water samples revealed that the V34 and V4 primer sets were the optimal choices. The 16S analysis comprised QIIME1: q1 and QIIME2: qII, with qII redesigned for clustering the amplicon sequence variant's operational taxonomic units (OTUs) [42]. Alpha-diversity, represented by the Shannon indexes, Simpson indexes, was estimated based on the amplicon sequence variant profiles from 16S rRNA sequences.

### *2.4. Health Risks Assessment*

In this section, a visual mapping of the bacterial and fungal aerosol spread was conducted, based on a graphic program of the distribution of air-transmitted bioaerosols. Bioaerosol induced risks in the study areas were simulated using CFD modelling. The details of the CFD modelling are given in the supplementary information. The model predicted bioaerosol concentration was delineated and hierarchically categorized using the Quantitative Microbial Risk Assessment methodology alongside DNA sequencing results [43,44]. The quantitative microbial risks were assessed using Equations (1) and (2):

$$Dose = C_c \times I \times t \quad (1)$$

$$P_r\,(Dose, t) = 1 - e^{-k \times Dose} \quad (2)$$

where *Dose* denotes the exposure concentration (CFU/m$^3$), $C_c$ refers to the cultivable pathogenic microbe concentration in the air (CFU/m$^3$), $I$ is the inhalation rate (m$^3$/h), and $t$ represents the exposure time (h) [45]. Inhalation rates increase when undertaking vigorous activities and during exercise [46]. Here, $I$ was set to 1.2 (light-intensity duties), 2.2 (moderate-intensity duties), and 3.2 (high-intensity duties), and $t$ was assumed to be 8 h. In addition, the probability of infection varied nonlinearly depending on the type of respiratory PM to which a person is exposed [47]. In the present study, the probability of infection $P_r$ was calculated using a dose-response relationship. Subsequently, $k$, which denotes the survival probability of a single gram-negative bacillus pathogen, was set to $3.52 \times 10^{-6}$ [48].

## 3. Results

### *3.1. Airborne Bioaerosol Concentration Profiles*

Landscape structure is a key driver of microbial biogeographic patterns [49]. While the concepts of "the environment selects" and "the microbe is everywhere in the biosphere" are widely accepted, there has been less consideration given to the impact of the built environment [50–52]. Hence, the artificial surface area ($I_{artificial\text{-}land}$), which is a function of the microbial concentration due to environmental drivers and population mobility, and the natural surface area ($II_{natural\text{-}land}$), which is a key driver of microbial transmission profiles under environmental stresses, we are studied here. In each city, an Andersen sampler with six agar plates was used to monitor airborne bioaerosol concentrations on-site. The bioaerosol concentration C′ was determined from BAP from 7 sampling sites ($I_{artificial}$: GTZ, NT, WAD, YL; $II_{natural}$: FSSK, NDH, YMT) in FX and the results were compared with microbial counts obtained using a NAP. At GTZ, NT, and WAD, the bioaerosol concentrations were 176, 308, and 87 CFU/6-plate (2073 CFU/m$^3$, 3628 CFU/m$^3$ and 1025 CFU/m$^3$), respectively, while the concentrations in the FSSK, NDH, and YMT were 69, 43, and 157 CFU/6-plate (813 CFU/m$^3$, 506 CFU/m$^3$ and 671 CFU/m$^3$), as shown in Figures 2a–c, and e–g. The average bioaerosol concentration in $I_{artificial}$ areas was found to be many times higher than in $I_{natural}$ areas. This implies that anthropogenic factors significantly affected the spatial distribution of microbes.

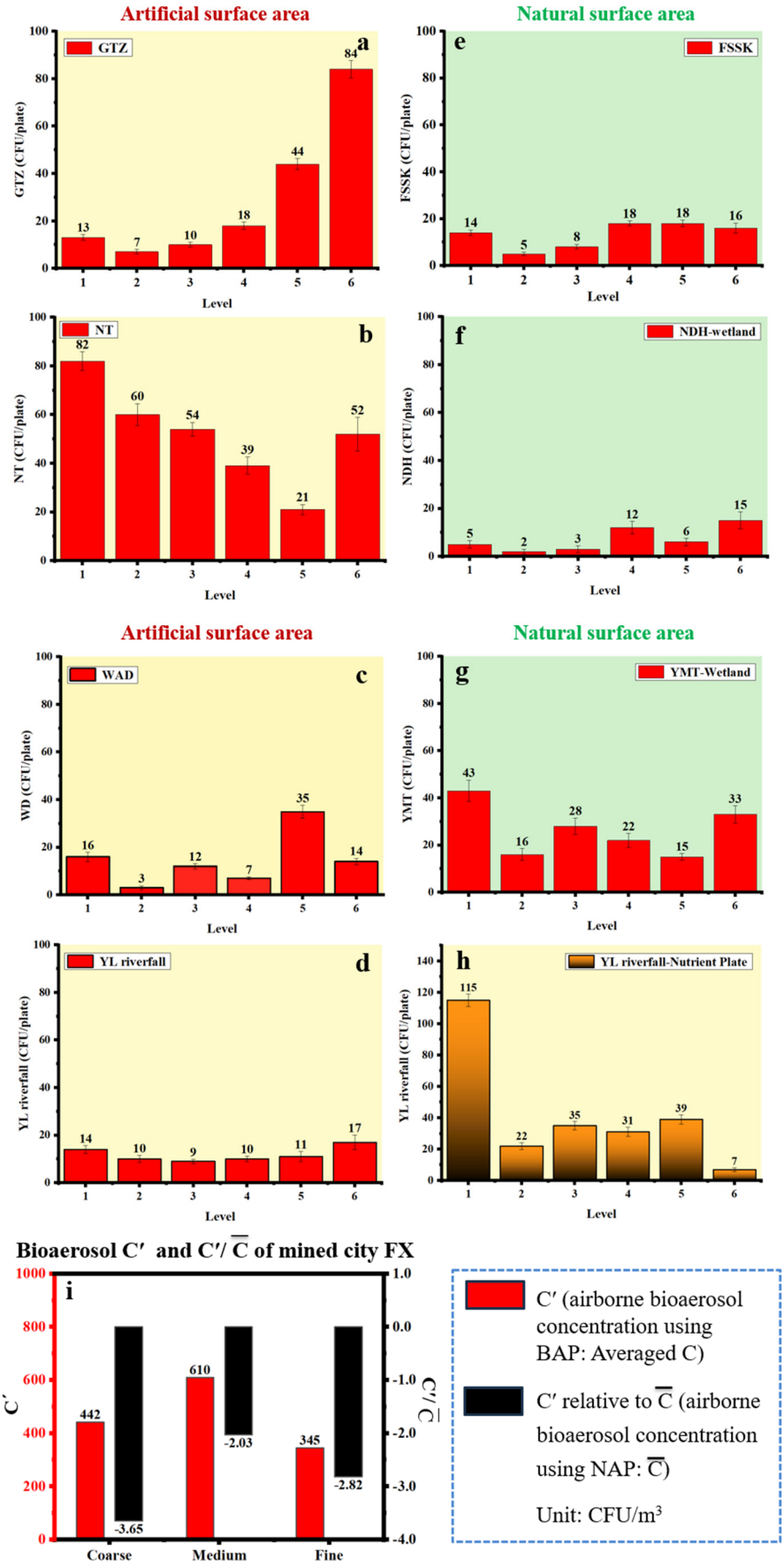


**Figure 2.** Airborne microbial concentration in the artificial and natural surface areas using the BAP and the NAP method: (**a**) GTZ; (**b**) NT; (**c**) WAD; (**d**) the YL riverfall; (**e**) and the FSSK wetland; (**f**) the NDH wetland; (**g**) the YMT wetland using the BAP; and (**h**) the YL riverfall using NAP; (**i**) the total averaged bioaerosol concentration ratio in FX.

Moreover, as shown in Figure 2d,h, the concentrations of airborne bioaerosol using NAP, and BAP in the YL river fall area were 249 CFU/6-plate and 71 CFU/6-plate (2933 CFU/m$^3$ and 836 CFU/m$^3$), respectively, which accounted for 28.5% of the ambient pathogenic bioaerosol concentration. In the mining city (FX), the bioaerosol concentration exceeded the safe inhalation exposure limit (≤500 CFU/m$^3$). Furthermore, the averaged C, which also named as C′ (airborne bioaerosol concentration using BAP, which is also designated as averaged C) and C′/$\bar{C}$ (airborne bioaerosol concentration using NAP is designated as $\bar{C}$) were compared, as shown in Figure 3i. It was found that the concentration of cultivable pathogenic bioaerosol was consistently lower than the concentration of bioaerosol. Based on the averaged concentration of medium-sized bioaerosol was also abundant in the air of FX.

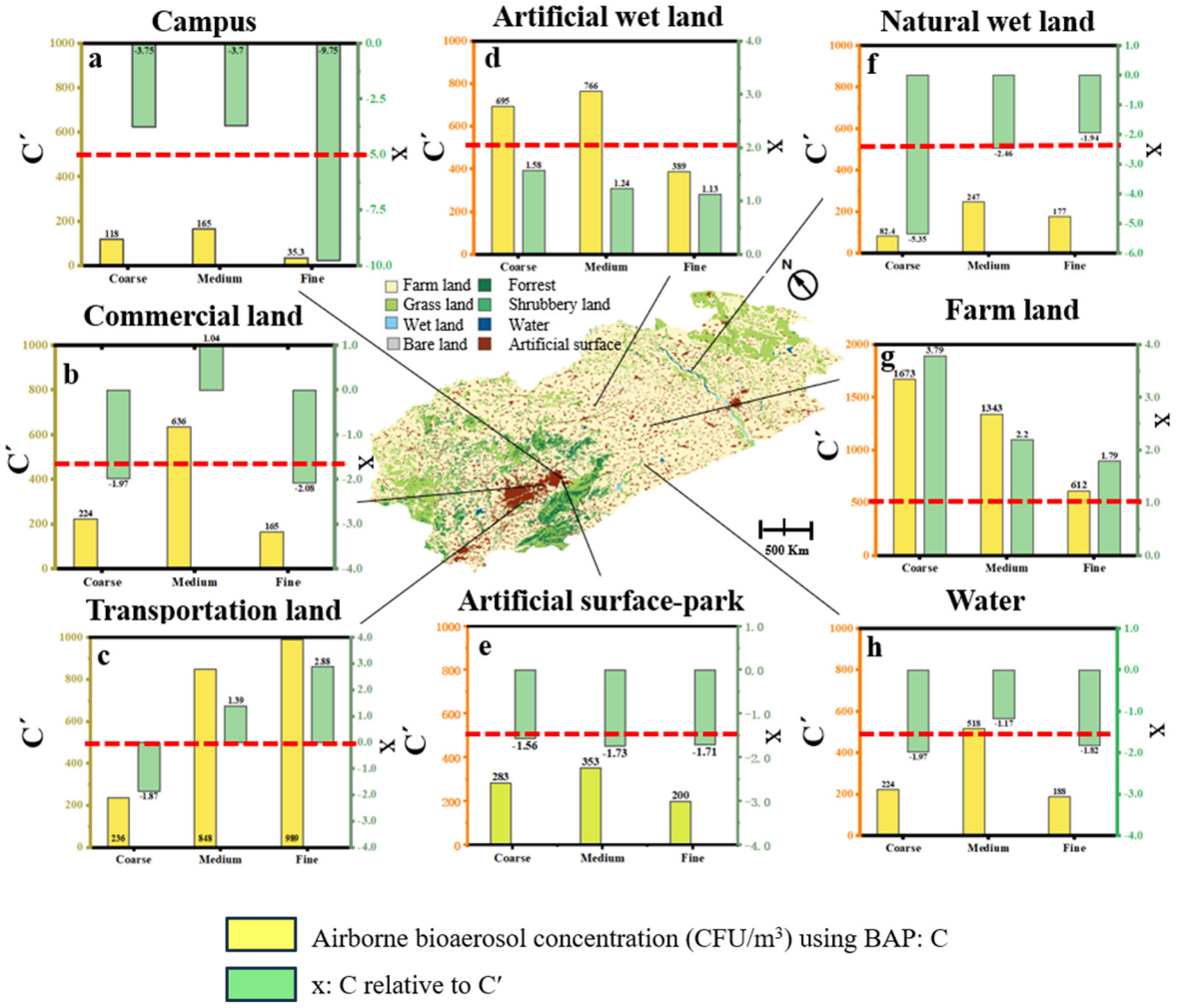


**Figure 3.** Size and concentration of bioaerosols in the air, water, and soil in FX at sampling sites in the: (**a**) campus; (**b**) commercial land; (**c**) transportation land; (**d**) artificial wetland; (**e**) artificial park; (**f**) natural wetland; (**g**) farmland; and (**h**) water taken close to the shore side of a water body.

The bioaerosol diameters in the mining city (FX) were also measured. There were high bioaerosol concentration in areas with a high intensity of human activities. For instance, at GTZ, fine airborne bioaerosols (0.65–3.3 μm) accounted for 83% of the total bioaerosol; while at NT, coarse airborne bioaerosols (>3.3 μm) accounted for 64% of the total concentration. Nonetheless, the concentration of bioaerosol was low in the natural land use regions. For example, at FSSK (a water reservoir), the airborne bioaerosol concentration was low and fine bioaerosols (0.65–3.3 μm) accounted for 64% of the total concentration. At NDH, coarse airborne bioaerosols (>3.3 μm) accounted for 23% of the total bioaerosol concentration.

As shown in Tables S1 and S2, it was found that high PM concentrations did not correspond to high bioaerosol concentrations. For example, at GTZ, the $PM_{1.0/2.5/10}$ concentrations were low at 12, 25, and 33 μg/m$^3$, respectively, while the bioaerosol concentration (0.65–1.1 μm) was 989 CFU/m$^3$, accounting for 57% of the total PM concentration; and the bioaerosol concentration (>7.0 μm) was 153 CFU/m$^3$, accounting for 9% of the total PM concentration. At FSSK, the $PM_{1.0/2.5/10}$ concentrations were high at 63, 103, and 169 μg/m$^3$, respectively, while the fine bioaerosol concentration (0.65–1.1 μm) is 188 CFU/m$^3$, accounting for 20% of the total

concentration; and the bioaerosol concentration (>7.0 μm) was 165 CFU/$m^3$, accounting for 18% of the total concentration. These results revealed that other than the relationship between the bioaerosol and particle concentrations, the size distribution of aerosols differed significantly, with implications for both air quality and climate change [26]. Therefore, it was inferred that regional air quality could not overshadow the effects of local anthropogenic aerosol emissions originating from various sectors within mining cities. To further highlight the regional concentration characteristics of bioaerosol concentration, the fluctuations in the concentrations of coarse- (>4.7 μm), medium- (2.1–4.7 μm) and fine- (0.65–2.1 μm) sized bioaerosols in the atmosphere were determined.

### *3.2. Bioaerosol Concentration Ratios Under Different Land Use*

Potential pathogens are present in PM when there are high concentrations of airborne bioaerosols. In this section, Figure 3 shows the bioaerosol concentration (yellow bar) cultured by BAP, assigned as C, and a concentration ratio of bioaerosol (x: C/C′) (green bar) columns of 7 different categories of land use. C′ and $\bar{C}$ represent average airborne bioaerosol concentrations using BAP, and NAP, respectively. The suggested safe concentrations of bioaerosol (500 CFU/$m^3$ medium limit) set by the European Commission, American Conference of Governmental Industrial Hygienists and World Health Organization were reached at the majority of sites and is shown by the red dotted line in the figure [53]. The total concentrations of airborne bioaerosols (coarse, medium, and fine) were 118, 165, and 35 CFU/$m^3$ at the campus site. This indicated that neither bacterial bioaerosol levels, nor dust concentrations exceeded the permissible values provided by bioaerosol pollution guidelines. In commercial land and transportation land, the coarse bioaerosol concentration did not exceed the permissible level. Densely populated areas were exceptions, with medium and fine bioaerosol concentrations in transportation land, commercial land, and artificial wetland being extremely high, with some samples exceeding 1000 CFU/$m^3$. Furthermore, the coarse and medium bioaerosol concentrations in farm land were 1673 CFU/$m^3$ and 1343 CFU/$m^3$, respectively, which implied that these aerosols made significant contributions to urban air pollution.

The China Scientific Ecology Centre, recommends a guideline value of <1000 CFU/$m^3$ for total airborne bacteria and <500 CFU/$m^3$ for airborne fungi in outdoor environments [54]. Because densely populated areas are a major source of bioaerosol, more attention should be given to their thorough cleaning. The concentration ratio of airborne pathogenic bioaerosol (x) was determined and characteristic distribution patterns were observed in the mining city (FX). For example, sampling sites in the farm land ($I_{artificial\text{-}farm\text{-}land}$) had the highest ratios of 3.79 for coarse particles, while the sampling site in the campus ($I_{artificial\text{-}campus}$) had the lowest ratio of −3.75. In the artificial land use types, the bioaerosol concentration ratio was lowest for fine particles at the campus site. Because fine bioaerosols have higher inhalation and infection risks, further investigations of ambient bioaerosol richness and community diversity were conducted to assess the potential infection risks. This was conducted via a sequencing analysis. Furthermore, in artificial land sites, the fine pathogenic bioaerosol concentration was high. For example, the highest concentration of 989 CFU/$m^3$ was found for transportation land (GTZ) (Figure 3c), while the fine pathogenic bioaerosol concentration was lower in the natural wet land area (FSSK) at 177 CFU/$m^3$ (Figure 3f).

### 3.3. *Characteristics of the Bioaerosol Community*

Biological diversity, a multidimensional property of natural systems, is difficult to quantify in the external environment of large cities. In this study, high-throughput sequencing data were analyzed, as shown in Figure 4. Operational taxonomic units (OUTs), are widely used as a fundamental analytical unit to describe biological communities through the amplicon sequencing of the 16s rRNA gene in microbial ecology studies [55]. The visualization of OTUs in environmental samples depicts the relative abundance of individual taxa in a set of samples on multiple taxonomic levels [56]. In this section, the OTU numbers at FSSK (FX) and HD (GZ) were comparatively analyzed, as shown in Figure 4a,b. The numbers of bacterial OTUs in the air, water, and soil samples were 1511, 1512, and 1485 in the 40,000 number sequences at FSSK in FX, while the corresponding numbers were 1017, 1299, and 1507 at HD in GZ. Furthermore, in the 40,000 number sequences at FSSK in FX, the fungal OUT numbers in the air, water, and soil achieved 781, 681, and 662, respectively. The corresponding numbers at HD in GZ were 392, 347, and 253, respectively. Therefore, there were large differences in the diversity of species (bacteria and fungi) between the two cities.

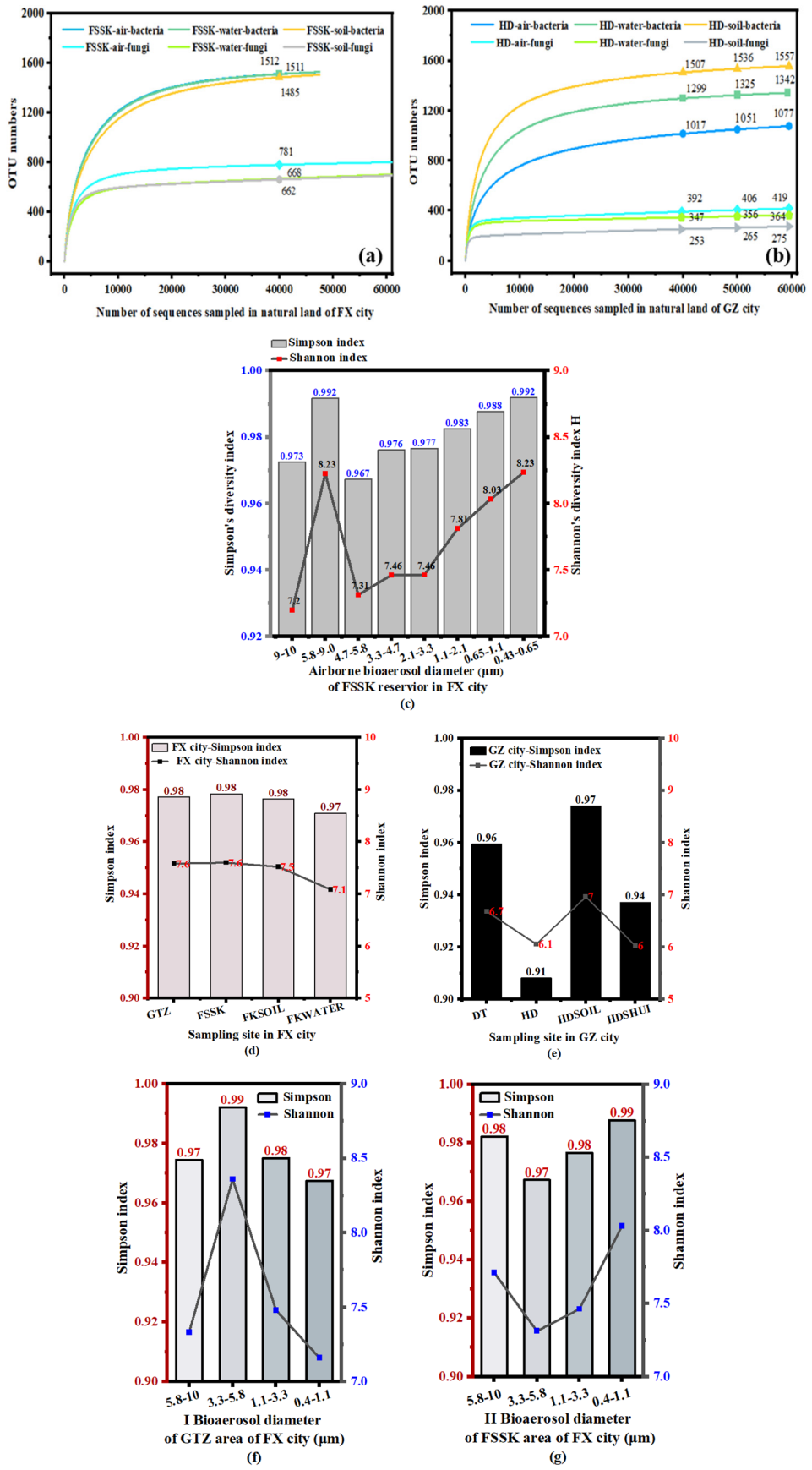


**Figure 4.** The diversity of urban outdoor environmental bioaerosols: (**a**,**b**) OUT numbers profile; (**c**) Simpson's diversity index and Shannon's diversity index of 8 size-ranged bioaerosols in FSSK wetland in FX city; (**d**) diversity indexes of airborne bioaerosols at GTZ, and FSSK, and in water (FKWATER), soil (FKSOIL) of FSSK in FX; (**e**) diversity indexes of airborne bioaerosols at DT and HD, and in water (HDSHUI), soil (HDSOIL) at HD in GZ; and (**f**,**g**) the differences between the diversity of airborne bioaerosols from FSSK wetland and GTZ in FX.

As key metrics of urban environmental species diversity-species richness, the Shannon and Simpson indexes are widely used for determining community diversity [57]. The Simpson index is a measure of probability; the greater the index value, the less likely it is that two randomly chosen individuals will belong to the same species. The Shannon diversity index H has a value of H ranges from 0 to a maximum that depends on the number of species and their distribution within a given community. The index, is related to the concept of uncertainty and takes into account both species richness and evenness. The maximum value of H is different for each community and is dependent on the species richness. In Figure 4c, there are eight size ranges of bioaerosols. The sequencing technique demonstrated that the specific size of a bioaerosol influenced its Simpson's diversity index and Shannon's diversity index H. For instance, at FSSK reservoir in FX, 0.43–1.65 μm bioaerosol size class had a Simpson diversity index value of 0.992 and a Shannon diversity index H of 8.23. Whereas, for the 9–10 μm size stage, the coarse-sized bioaerosol had a H value of 7.2, which was 87% higher than that of fine bioaerosols. It was concluded that even if there was homogenous distribution of biological species in mining cities, the fine bioaerosols may contain a greater diversity of airborne bacteria and fungi.

In Figure 4d,e, although the airborne bacteria bioaerosol sampling sites in the artificial land (GTZ and DT) had relatively high diversity index values (GTZ: Simpson index: 0.98, Shannon index:7.6; DT site: Simpson index: 0.96, Shannon index: 6.7), the airborne bioaerosol diversity in the natural land (the FSSK and HD site) was significantly different (FSSK site: Simpson index: 0.98, Shannon index:7.6; HD site: Simpson index: 0.91, Shannon index: 6.1). Compared to the air and water samples, there was a higher bacterial diversity in the soil in GZ. In a Venn diagram of the results, the number in the inner of the flower is 47, which indicates the mutually characterized number; while the outer of the flower at FSSK, GTZ and HD, DT site air was 94, 27 and 27, 40, highlighting the unique characterized number, except for that of FSSK-air. Then, the diversity at FSSK and the GTZ merits additional comparison. Figure 4f, g shows that airborne bioaerosols in the 5.8–10, 3.3–5.8, 1.1–3.3, and 0.4–1.1 μm size stage at GTZ (an $I_{artificial\text{-}land}$ area) had Simpson index of 0.97, 0.99, 0.98 and 0.97, respectively; while at FSSK (an $II_{natural\text{-}land}$ area) had Simpson index values of 0.98, 0.97, 0.98 and 0.99. From these results it was determined that 3.3–5.8 μm size stage were the most diverse in both artificial land and natural land areas. Table S3 shows that the Simpson and Shannon index values for air samples at HD were 5.2% lower than those DT (a metro station) in GZ, however, the inverse trend was apparent in FX. The air samples from FSSK and GTZ displayed peak and valley curve distributions for airborne bioaerosol sizes, and species diversity, particularly in the natural land sites.

### *3.4. Size, Concentration, and Composition Differences of Urban Bioaerosls*

The physical and chemical characteristics of micron-sized PM (such as coal mining dust) in ambient air have been extensively studied, however, little information exists for its biological components [58]. In the present study, bioaerosol dynamics (size, concentration, and species composition) were determined for samples taken at various urban locations with different monsoon climate. Figure 5a showed that in in FX with a warm monsoon climate, fine bioaerosols (<2.1 μm) were abundant, with a metro station (GTZ) having a bioaerosol (0.65–>7.0) concentration of 2073 CFU/$m^3$. Park and river/wet land areas also exhibited high bioaerosol concentrations (813 CFU/$m^3$ and 836 CFU/$m^3$). Figure 5b shows that in GZ with subtropical monsoon climate, small-sized bioaerosols (<2.1 μm) were also abundant. A bioaerosol (0.65–>7.0) concentration of 412 CFU/$m^3$ was found at a transportation land area (DT, a metro station). The bioaerosol concentration in an outdoor activity area in a location with a high population density (P, a country park) was 565 CFU/$m^3$. Ascomycota, Basidiomycota and Chytridiomycota had high relative abundance (>62%) at DT and HD in GZ, as shown in Figure 5c. However, their relative abundance has relatively low value (<59%) at both FSSK and GTZ in FX. Overall, the high relative abundance (>98%) of the top 5 fungal species in the 2 cities resulted in a similar community structure (Ascomycota, Basidiomycota, Chytridiomycota, unclassified_Fungi, Mortierellomycota).

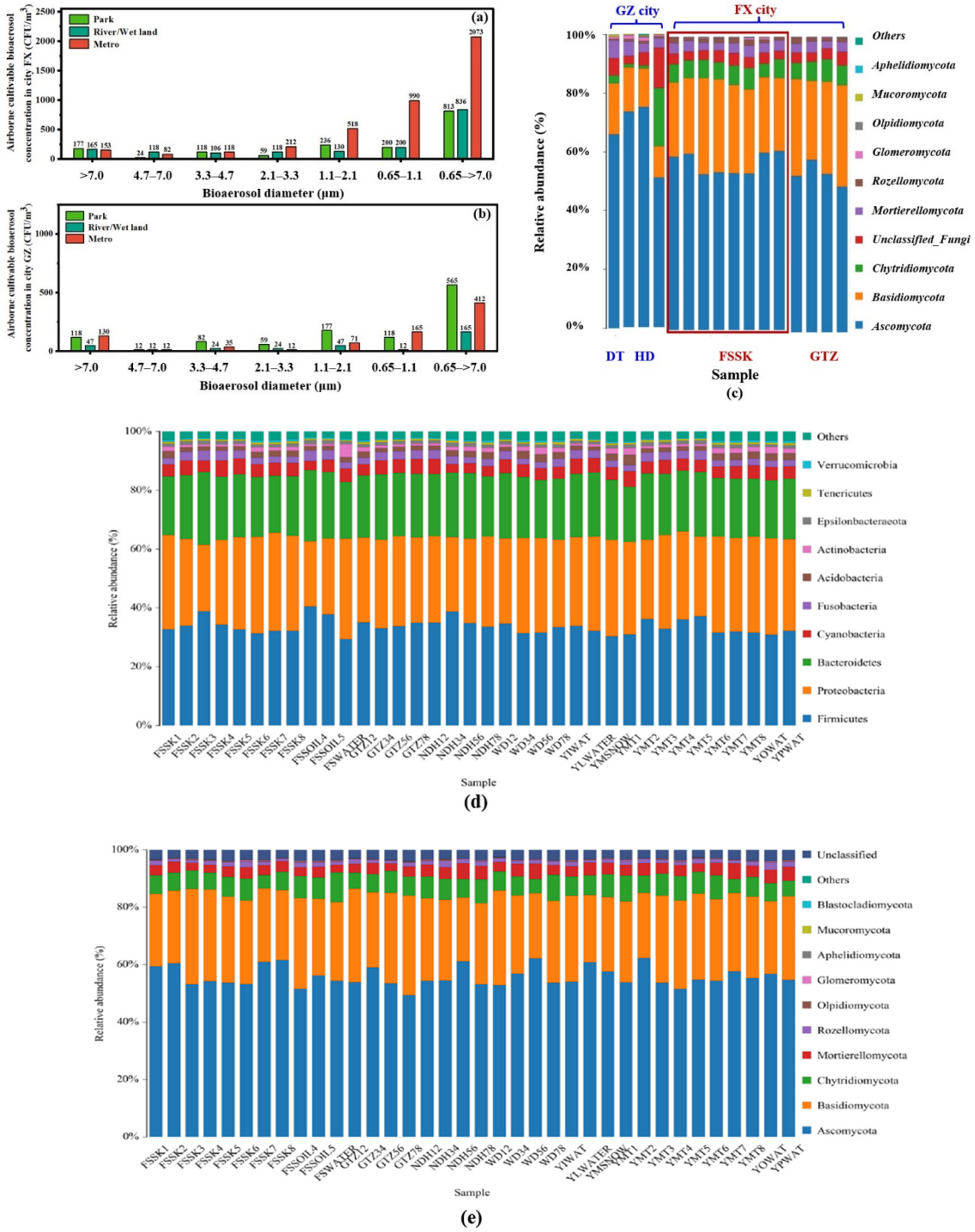


**Figure 5.** Cultivable bioaerosol composition, size and concentration distribution in two cities, FX and GZ: (**a**,**b**) size and concentration distribution of the cultivable bioaerosol composition; (**c**) top 10 fungal bioaerosols in the two cities; and (**d**,**e**) top 10 bioaerosol relative abundance of bacteria and fungi in the 35 sampling sites in FX.

Figure 5d,e further shows the bacterial and fungal composition in 36 samples using the 3rd generation DNA sequencing platform. The results indicated that the top 3 species are similar. For instance, the top 3 bacterial species are Firmicutes, Proteobacteria and Bacteroidetes; while the top 3 fungal species were Ascomycota, Basidiomycota, and Chytridiomycota. However, there was evidence that airborne bioaerosol species with different sizes had different relative abundances. To fully assess this, FSSK was used as a case study, with the number after the results representing the level of the 8-staged Anderson sampler. For instance, FSSK3 has a high relative abundance (40%) of Firmicutes; FSSK1, FSSK2, FSSK7, and FSSK8 have a high relative abundance (61 ± 1%) of Ascomycota. Moreover, an abundance of cultivable fungi and bacteria were detected through the rDNA sequencing technique. A large number of pathogens including *Streptococcus pneumoniae*, *Bacillus cereus*, *Prescottella equi*, *Escherichia*

*coli*, and *Aspergillus fumigatus* were presented in FX, as shown in Table S4. These results indicated that there were characteristic microorganisms in different sized bioaerosols at specific sites in both cities, involving abundant fungal and bacterial entities, and therefore more depth risk assessment studies are required in the future.

### *3.5. Regional Risk Prediction and Infectious Potential Modelling*

For biogeochemical studies, it would be useful to access more detailed information on different types of particles and their associated biological composition [59]. However, stiff and inert spherical particles are commonly employed in modelling the dispersion of biological dust dispersion modeling. Documenting the spatial patterns in biodiversity-induced bioaerosol characteristics is difficult due to the limited quantification of taxonomic information, health risks, and other dimensions of risk. This highlights the need for multiple sources of in-situ data to address these gaps effectively [60]. Inhalation was the main exposure route for pathogenic bioaerosols, with the exposure risks linked to the inhalation route being more than $10^5$ times greater than those associated with the dermal contact route for both children and adults [61]. Bioaerosol distribution modelling in the artificial land area was conducted based on the on-site measured airborne bioaerosol concentration, size and composition.

As indicated in Figure S1 shows PM with specific cultivable bacteria and fungi are abundant, and there were high frequences of the dominant Gram+ bacteria, including *Bacillus cereus* and *Staphylococcus epidermidis*, and fungi, involving *Aspergillus fumigates*, and *Aspergillus awamori*, occur. The details of the meteorological parameters during the on-site monitoring of the cultivable bacteria and fungi at the campus in FX given in Table S5. From the on-site monitoring data, ï was recalculated as 0.95 CFU/μg. The mass concentration of PM was set to 255 μg/m$^3$, while the airborne cultivable bioaerosol concentration was 225 CFU/m$^3$. This was used to transform the mass concentration of aerosol ($C_m$, μg/m$^3$) and bioaerosol ($C_c$, CFU/m$^3$) based on an in-situ data-derived Equation (3).

$$C_c = C_m \times ï \times 10^9 \quad (3)$$

where ï is a transform coefficient with a unit of CFU/μg.

Consequently, it was possible to anticipate the related risks and infectious potential numerically. And then, the boundary conditions set for the winter of FX are presented in Table S6. Furthermore, Table S7 gives the details of the setups of the CFD-based bioaerosol concentration distribution contours and associated risk predictions.

The modelling-based bioaerosol distribution at GTZ in FX is shown as a schematic Figure 6a,b. At a typical wind speed of 0.25 m/s, there was a noticeable shift in the direction of atmospheric diffusion, which influenced the distribution patterns observed on building surfaces. At DT in GZ and GTZ in FX, the distinct building structure patterns corresponded to distinct patterns of atmospheric diffusion, thus influencing the bioaerosol concentrations. For example, the average airborne bioaerosol concentration in GZ, at 1.5 m surface height and over a 720-s emission period, was 9 CFU/m$^3$ (Figure 6b), while the average concentration at sites in FX reached 64 CFU/m$^3$ (Figure 6a). The potential infectious dose at GTZ in FX and DT in GZ is presented in Figure 6c, d under a weak wind speed (2.5 m/s) and a northerly N wind direction. For instance, the area-weighted average concentration of airborne bioaerosol at DT in GZ was 4 CFU/m$^3$ over a comparative emission period, as shown in Figure 6d. In contrast, the concentration at GTZ in FX reached 5 CFU/m$^3$ with a wider range of bioaerosol concentrations, as shown in Figure 6c. Wider diffusion ranges and comparatively larger concentrations of bioaerosol were observed in the populated area of FX.

Aerosols containing infectious pathogens have a significant impact on human health and safety [62,63]. The CFD modeling aerosols as well as risk model calculation have been promoted to estimate community infection levels. Modelling can be simplified by considering pathogenic bioaerosols in the air [64]. In the present study, the outdoor infection probability distribution of pathogenic bioaerosols in the surface air at GTZ in FX and DT in GZ are shown in a scheme in Figure 6(e1–e3,f1–f3). The bioaerosol concentrations distribution varied in the 2 km region surrounding the transportation buildings. These airborne cultivable bioaerosol dose distribution contours suggested that high-intensity duties could lead to a higher inhalation rate at GTZ and DT, as schemed in Figure 6(e3,f3). Furthermore, high concentration of pathogens would likely be present in similar areas, which would lead to higher pathogen doss. The wider concentration distribution ranges and borders were related to the wind-intensified diffusion in the street canyons of urban areas, which resulted in longer resident time and doses around the transportation hubs. These doses could also vary substantially with individual differences, respiratory activities, and activity levels.

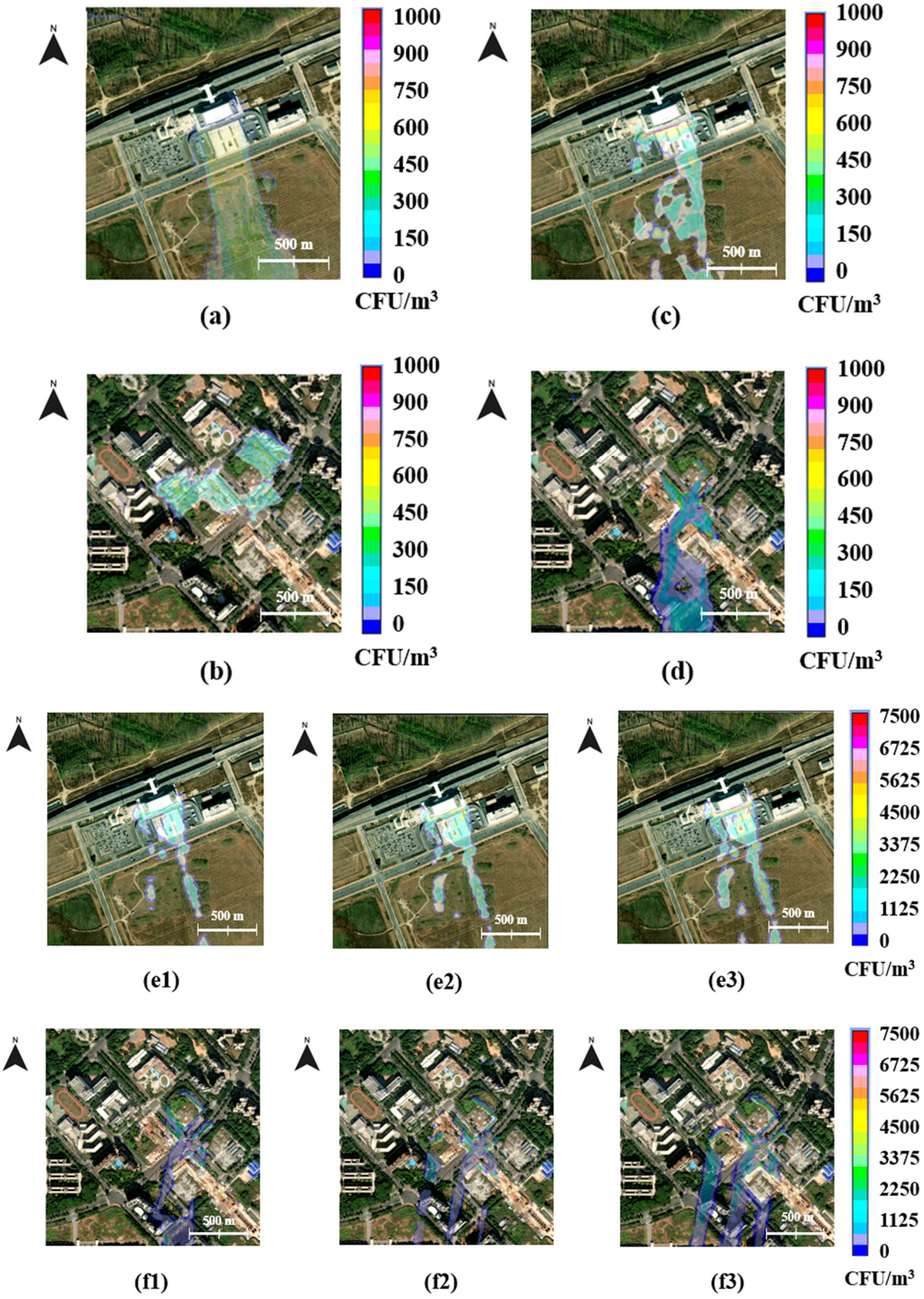
N
500 m
1000
900
750
600
450
300
150
0
CFU/m³
(a)
(c)
(b)
(d)
7500
6725
5625
4500
3375
2250
1125
(e1)
(e2)
(e3)
(f1)
(f2)
(f3)

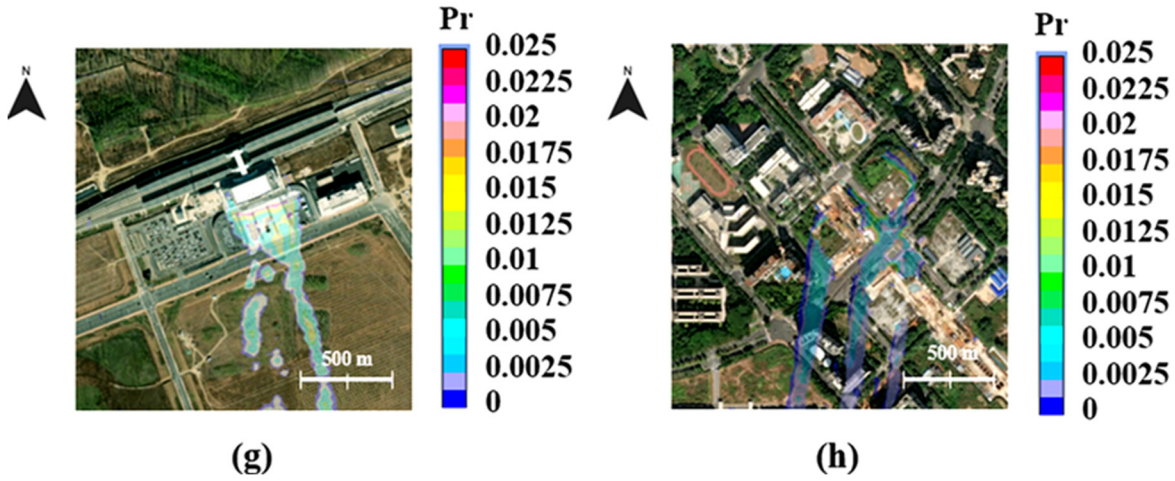


**Figure 6.** (**a**,**b**) Bioaerosol diffusion risks profiles, and bioaerosol concentration distribution patterns at a wind speed of 0.25 m/s at GTZ in FX and DT in GZ; (**c**,**d**) diffuse bioaerosol inhalation risks at GTZ and DT at a wind speed of 2.5 m/s; (**e1**–**e3**) and (**f1**–**f3**) bioaerosol inhalation risks and the infectious dose at GTZ and DT area, respectively; (**g**,**h**) contours in different transportation infrastructures in FX and GZ under light-, moderate-, and high-intensity activities.

In this study, the CFD-based risk prediction conducted here further demonstrated the fact that, under a weakened wind speed (2.5 m/s), the pathogenic bioaerosols are more mixed and dispersed, presenting un-uniformly infection potential distribution of several examples in the high-density populated areas. For instance, human busy activity produced a broader inhalation dose distribution of pathogenic bioaerosols in the railway station (GTZ) and the subway station (DT) (Figure 6e3,f3), and subsequently, the infection potential Pr increased, as shown in Figure 6g,h. The locations with the highest Pr were determined to be in downwind regions with wider diffusion ranges. In a poorly ventilated street block, the probability of infection by airborne pathogens was greater in the outdoor environment. This newly proposed quantitative modelling process for determining the nature of bioaerosols demonstrated the probability of infection while also considering building structures and the distance between emission sources, and ultimately confirmed the importance of a pathogens' airborne transmission. For instance, the 1.5 m surface-averaged $P_r$ at GTZ in FX was 0.00038, while $P_r$ at DT area in GZ decreased to 0.00030. *Aspergillus fumigatus* abundant in the air samples during on-site monitoring, which confirmed the good performance of the risk assessment modelling. Thus, ambient aerosols, such as mine dust, carrying pathogenic microorganisms can serve as hazardous pollutants in cities. The presence of these microorganisms in PM increases the probability of human diseases, including invasive aspergillosis by *Aspergillus fumigatus*, and therefore cleaning procedures are necessary [65,66].

## 4. Discussion

Our findings suggest that the aggregation of pathogens on inhalable particles to form hazardous bioaerosols may play a significant role in the health risks presented by adverse atmospheric conditions in different cities. The regional climate forced ambient particle size distribution, reflects the diversity of emission sources in a region. It is associated with the formation of new urban particles during winter, which are characterized by rapid growth [67]. Through the on-site sampling of the atmosphere at artificial and natural land sites, we detected variations in the enhancement of the relationship between bacteria and fungi species abundance, and fine-, medium-, coarse-PM concentrations. These variations were largely due to the effects of regional atmospheric diffusion. Rapid urbanization and industrialization contribute to the complicated composition of biological particles in megacities, where particles are emitted from a source and are spread throughout the surrounding areas due to the action of the winds. As shown by the bioaerosol diffusion contours around the urban transportation infrastructures, the Pr distribution ranged between 0 and 0.01. The pathogen infection probability in airborne PM would likely increase in the downwind direction. Additionally, inhalable bioaerosols tend to remain in the vicinity of their emission sources, following outdoor atmospheric diffusion trajectories, which may be inhaled by individuals in the area.

## 5. Conclusions

The sources of bioaerosol and their characteristics, such as size, concentration, composition, cultivable clinical pathogens infection potential, as well as their associated implications were thoroughly studied. A large

number of environmental microorganisms were found to be present in air, soil and water samples taken from various locations in mining cities. The bioaerosol concentration exceeded the suggested safe inhalation exposure limit (<500 CFU/$m^3$) in artificial areas with intense human activities, including farm land and transportation station. In the winter, the composition of airborne bioaerosols was more homogenous than in other seasons. Under a warm monsoon climate situation, intense anthropogenic activity (such as coal mining) contributes to the diffusion of biological aerosols into the air, resulting in a bioaerosol exposure level of 2073 CFU/$m^3$. A wind speed of 2.5 m/s had a strong impact on air quality through mine dust resuspension, which intensify the effects of human activities on air quality in the mining region. A reduction in wind speed facilitated the transmission of airborne bioaerosol leading to the emergence of unexpected clinical pathogens within ranges comparable to those found in urbanized environments. Using the proposed observational data-validated modelling method, which integrates regional environmental modelling and ambient bioaerosol exposure dose prediction, together with an infection probability distribution, we were able to expand the capability of modellings to determine the risk presented by pathogenic bioaerosols in urban environments.

**Supplementary Materials:** Figures and tables that directly support the study design and outcome are submitted here as supplementary material. The following supporting information can be downloaded at: https://www.sciltp.com/journals/ges/2025/1/336/s1. Table S1: Air PM concentration and Meteorological data of sampling sites with 9 land use types in FX city. Table S2: Air PM concentration and meteorological data of sampling sites with 3 land use types in GZ city. Table S3: Diversity, richness and bacterial concentration of sampling sites within sampling area atmospheres in GZ city and FX city. Table S4: Airborne cultivable fungal and bacterial species information in aerosol in FX city in 2021. Table S5: On-site monitored airborne cultivable fungal and bacterial species information in aerosol in campus of FX city in the winter of 2022. Table S6: On-site monitored airborne cultivable fungal and bacterial species information-based simulation boundary settings and outputs in CFD. Table S7: Additional initial condition, operating condition and boundary condition of the GIS-CFD simulation in this study. Figure S1: Frequency of isolation of dominant cultivable bacterial and fungi species in air samples of FX city.

**Author Contributions:** T.Z.: conceptualization, experimentation, experimental setup development, computational analysis, algorithm development, methodology, validation, interpretation of data, data analysis, writing—original draft and editing. Y.C.: experimentation, experimental setup development, cell culturing. G.L.: conceptualization, project administration, writing—review & editing. All authors have read and agreed to the published version of the manuscript.

**Funding:** This work was supported by the National Natural Science Foundation of China (Nos. 42007385, 42130611), the Natural Science Foundation of Liaoning Provincial, China (No. 2023-MS-316), and the Talent Foundation of Liaoning Technical University, China (No. 21-1144).

**Conflicts of Interest:** The authors declare no conflict of interest.

## References

1. Winkler, K.; Fuchs, R.; Rounsevell, M.; Herold, M. Global land use changes are four times greater than previously estimated. *Nat. Commun.* **2021**, *12*, 2501.
2. Dadashpoor, H.; Azizi, P.; Moghadasi, M. Land use change, urbanization, and change in landscape pattern in a metropolitan area. *Sci. Total Environ.* **2019**, *655*, 707–719.
3. Zhou, W.; Yu, W.; Qian, Y.; Han, L.; Pickett, S.T.A.; Wang, J.; Li, W.; Ouyang, Z. Beyond city expansion: Multi-scale environmental impacts of urban megaregion formation in China. *Natl. Sci. Rev.* **2022**, *9*, nwab107.
4. Espey, J.; Parnell, S.; Revi, A. The transformative potential of a Global Urban Agenda and its lessons in a time of crisis. *NPJ Urban Sustain.* **2023**, *3*, 15.
5. Pandey, B.; Brelsford, C.; Seto, K.C. Infrastructure inequality is a characteristic of urbanization. *Proc. Natl. Acad. Sci.* **2022**, *119*, e2119890119.
6. Yu, H.; Zahidi, I. Environmental hazards posed by mine dust, and monitoring method of mine dust pollution using remote sensing technologies: An overview. *Sci. Total Environ.* **2023**, *864*, 161135.
7. Maus, V.; Giljum, S.; Gutschlhofer, J.; da Silva, D.M.; Probst, M.; Gass, S.L.B.; Luckeneder, S.; Lieber, M.; McCallum, I. A global-scale data set of mining areas. *Sci. Data* **2020**, *7*, 289.
8. Worlanyo, A.S.; Jiangfeng, L. Evaluating the environmental and economic impact of mining for post-mined land restoration and land-use: A review. *J. Environ. Manag.* **2021**, *279*, 111623.
9. Sonter, L.J.; Ali, S.H.; Watson, J.E.M. Mining and biodiversity: Key issues and research needs in conservation science. *Proc. R. Soc. B Biol. Sci.* **2018**, *285*, 20181926.
10. Hara, K.; Zhang, D. Bacterial abundance and viability in long-range transported dust. *Atmos. Environ.* **2012**, *47*, 20–25.
11. Zhang, T.; Chen, Y.; Cai, Y.; Yu, Y.; Liu, J.; Shen, X.; Li, G.; An, T. Abundance and cultivable bioaerosol transport from a municipal solid waste landfill area and its risks. *Environ. Pollut.* **2023**, *320*, 121038.
12. Xie, Z.; Fan, C.; Lu, R.; Liu, P.; Wang, B.; Du, S.; Jin, C.; Deng, S.; Li, Y. Characteristics of ambient bioaerosols during haze episodes in China: A review. *Environ. Pollut.* **2018**, *243*, 1930–1942.
13. Li, Z.; Ma, Z.; van der Kuijp, T.J.; Yuan, Z.; Huang, L. A review of soil heavy metal pollution from mines in China: Pollution and health risk assessment. *Sci. Total Environ.* **2014**, *468–469*, 843–853.
14. Fan, P.; Lu, X.; Yu, B.; Fan, X.; Wang, L.; Lei, K.; Yang, Y.; Zuo, L.; Rinklebe, J. Spatial distribution, risk estimation and

source apportionment of potentially toxic metal(loid)s in resuspended megacity street dust. *Environ. Int.* **2022**, *160*, 107073.
15. Šantl-Temkiv, T.; Sikoparija, B.; Maki, T.; Carotenuto, F.; Amato, P.; Yao, M.; Morris, C.E.; Schnell, R.; Jaenicke, R.; Pöhlker, C.; et al. Bioaerosol field measurements: Challenges and perspectives in outdoor studies. *Aerosol Sci. Technol.* **2020**, *54*, 520–546.
16. Akimbekov, N.S.; Digel, I.; Tastambek, K.T.; Marat, A.K.; Turaliyeva, M.A.; Kaiyrmanova, G.K. Biotechnology of Microorganisms from Coal Environments: From Environmental Remediation to Energy Production. *Biology* **2022**, *11*, 1306.
17. Labouyrie, M.; Ballabio, C.; Romero, F.; Panagos, P.; Jones, A.; Schmid, M.W.; Mikryukov, V.; Dulya, O.; Tedersoo, L.; Bahram, M.; et al. Patterns in soil microbial diversity across Europe. *Nat. Commun.* **2023**, *14*, 3311.
18. Wanjun, T.; Qingxiang, C.A.I. Dust distribution in open-pit mines based on monitoring data and fluent simulation. *Environ. Monit. Assess.* **2018**, *190*, 632.
19. Wu, T.; Boor, B.E. Urban aerosol size distributions: A global perspective. *Atmos. Chem. Phys.* **2021**, *21*, 8883–8914.
20. Chen, P.-C.; Lin, Y.-T. Exposure assessment of PM2.5 using smart spatial interpolation on regulatory air quality stations with clustering of densely-deployed microsensors. *Environ. Pollut.* **2022**, *292*, 118401.
21. Faisal, A.-A.; Rahman, M.M.; Haque, S. Retrieving spatial variation of aerosol level over urban mixed land surfaces using Landsat imageries: Degree of air pollution in Dhaka Metropolitan Area. *Phys. Chem. Earth Parts A/B/C* **2022**, *126*, 103074.
22. Liu, L.; Zhang, X.; Gao, Y.; Chen, X.; Shuai, X.; Mi, J. Finer-Resolution Mapping of Global Land Cover: Recent Developments, Consistency Analysis, and Prospects. *J. Remote Sens.* **2021**, *2021*, 5289697.
23. Zhao, Y.; Zhu, Z. ASI: An artificial surface Index for Landsat 8 imagery. *Int. J. Appl. Earth Obs. Geoinf.* **2022**, *107*, 102703.
24. Zuo, J.; Rameezdeen, R.; Hagger, M.; Zhou, Z.; Ding, Z. Dust pollution control on construction sites: Awareness and self-responsibility of managers. *J. Clean. Prod.* **2017**, *166*, 312–320.
25. Edwards, D.P.; Sloan, S.; Weng, L.; Dirks, P.; Sayer, J.; Laurance, W.F. Mining and the African Environment. *Conserv. Lett.* **2014**, *7*, 302–311.
26. Li, J.; Carlson, B.E.; Yung, Y.L.; Lv, D.; Hansen, J.; Penner, J.E.; Liao, H.; Ramaswamy, V.; Kahn, R.A.; Zhang, P.; et al. Scattering and absorbing aerosols in the climate system. *Nat. Rev. Earth Environ.* **2022**, *3*, 363–379.
27. Sharma, R.; Kumar, A. Analysis of seasonal and spatial distribution of particulate matters and gaseous pollutants around an open cast coal mining area of Odisha, India. *Environ. Sci. Pollut. Res.* **2023**, *30*, 39842–39856.
28. Zhao, X.; Huang, J.; Lu, J.; Sun, Y. Study on the influence of soil microbial community on the long-term heavy metal pollution of different land use types and depth layers in mine. *Ecotoxicol. Environ. Saf.* **2019**, *170*, 218–226.
29. Zhang, J.; Fu, M.; Hassani, F.P.; Zeng, H.; Geng, Y.; Bai, Z. Land Use-Based Landscape Planning and Restoration in Mine Closure Areas. *Environ. Manag.* **2011**, *47*, 739–750.
30. Gutierrez-Velez, V.H.; Gilbert, M.R.; Kinsey, D.; Behm, J.E. Beyond the 'urban' and the 'rural': Conceptualizing a new generation of infrastructure systems to enable rural–urban sustainability. *Curr. Opin. Environ. Sustain.* **2022**, *56*, 101177.
31. Korek, M.; Johansson, C.; Svensson, N.; Lind, T.; Beelen, R.; Hoek, G.; Pershagen, G.; Bellander, T. Can dispersion modeling of air pollution be improved by land-use regression? An example from Stockholm, Sweden. *J. Expo. Sci. Environ. Epidemiol.* **2017**, *27*, 575–581.
32. Ma, X.; Gao, J.; Longley, I.; Zou, B.; Guo, B.; Xu, X.; Salmond, J. Development of transferable neighborhood land use regression models for predicting intra-urban ambient nitrogen dioxide ($NO_2$) spatial variations. *Environ. Sci. Pollut. Res.* **2022**, *29*, 45903–45918.
33. Ghosh, B.; Lal, H.; Srivastava, A. Review of bioaerosols in indoor environment with special reference to sampling, analysis and control mechanisms. *Environ. Int.* **2015**, *85*, 254–272.
34. Zhao, Y.; Zhang, J.; Wang, S.; Yu, L.; Yu, H.; Wang, Y.; Feng, L. Efficacy of 75% alcohol in pretreatment of the Andersen sampler in trapping maximum airborne microbes. *Aerobiologia* **2021**, *37*, 171–178.
35. Zhang, Z.; Wang, K. The Synoptic to Decadal Variability in the Winter Surface Wind Speed Over China by the Weather Regime View. *Geophys. Res. Lett.* **2021**, *48*, e2020GL091994.
36. Xu, Y.; Liu, Y.; Chen, R.; Meng, Y.; Li, K.; Fu, C. Study on the spatio-temporal evolution characteristics and driving mechanism of China's carbon emissions. *Humanit. Soc. Sci. Commun.* **2023**, *10*, 786.
37. Xu, M.; Chang, C.-P.; Fu, C.; Qi, Y.; Robock, A.; Robinson, D.; Zhang, H. Steady decline of east Asian monsoon winds, 1969–2000: Evidence from direct ground measurements of wind speed. *J. Geophys. Res. Atmos.* **2006**, *111*, D24111.
38. Mousavi, S.E.; Delgado-Saborit, J.M.; Adivi, A.; Pauwels, S.; Godderis, L. Air pollution and endocrine disruptors induce human microbiome imbalances: A systematic review of recent evidence and possible biological mechanisms. *Sci. Total Environ.* **2022**, *816*, 151654.
39. Wong, P.-Y.; Lee, H.-Y.; Chen, Y.-C.; Zeng, Y.-T.; Chern, Y.-R.; Chen, N.-T.; Candice Lung, S.-C.; Su, H.-J.; Wu, C.-D. Using a land use regression model with machine learning to estimate ground level PM2.5. *Environ. Pollut.* **2021**, *277*, 116846.
40. Xue, S.; Liu, X.; Li, Y.; Liu, B.; Tu, Q.; Li, C. Pathogenic Bacterial Communities of Dust in a Coal Mine. *Front. Environ. Sci.* **2022**, *10*, 857744.
41. Pincetl, S. Cities in the age of the Anthropocene: Climate change agents and the potential for mitigation. *Anthropocene* **2017**, *20*, 74–82.
42. Kameoka, S.; Motooka, D.; Watanabe, S.; Kubo, R.; Jung, N.; Midorikawa, Y.; Shinozaki, N.O.; Sawai, Y.; Takeda, A.K.; Nakamura, S. Benchmark of 16S rRNA gene amplicon sequencing using Japanese gut microbiome data from the V1–V2 and V3–V4 primer sets. *BMC Genom.* **2021**, *22*, 527.
43. Yang, K.; Li, L.; Xue, S.; Wang, Y.; Liu, J.; Yang, T. Influence factors and health risk assessment of bioaerosols emitted

from an industrial-scale thermophilic biofilter for off gas treatment. *Process Saf. Environ. Prot.* **2019**, *129*, 55–62.
44. Akila, M.; Earappa, R.; Qureshi, A. Ambient concentration of airborne microbes and endotoxins in rural households of southern India. *Build. Environ.* **2020**, *179*, 106970.
45. Lü, H.; Wen, S.; Feng, Y.; Wang, X.; Bi, X.; Sheng, G.; Fu, J. Indoor and outdoor carbonyl compounds and BTEX in the hospitals of Guangzhou, China. *Sci. Total Environ.* **2006**, *368*, 574–584.
46. Borghi, F.; Spinazzè, A.; Mandaglio, S.; Fanti, G.; Campagnolo, D.; Rovelli, S.; Keller, M.; Cattaneo, A.; Cavallo, D.M. Estimation of the Inhaled Dose of Pollutants in Different Micro-Environments: A Systematic Review of the Literature. *Toxics* **2021**, *9*, 140.
47. Cheng, Y.; Ma, N.; Witt, C.; Rapp, S.; Wild, P.S.; Andreae, M.O.; Pöschl, U.; Su, H. Face masks effectively limit the probability of SARS-CoV-2 transmission. *Science* **2021**, *372*, 1439–1443.
48. Medema, G.J.; Teunis, P.F.M.; Havelaar, A.H.; Haas, C.N. Assessment of the dose-response relationship of Campylobacter jejuni. *Int. J. Food Microbiol.* **1996**, *30*, 101–111.
49. Seppey, C.V.W.; Lara, E.; Broennimann, O.; Guisan, A.; Malard, L.; Singer, D.; Yashiro, E.; Fournier, B. Landscape structure is a key driver of soil protist diversity in meadows in the Swiss Alps. *Landsc. Ecol.* **2023**, *38*, 949–965.
50. Hanson, C.A.; Fuhrman, J.A.; Horner-Devine, M.C.; Martiny, J.B.H. Beyond biogeographic patterns: Processes shaping the microbial landscape. *Nat. Rev. Microbiol.* **2012**, *10*, 497–506.
51. Martiny, J.B.H.; Bohannan, B.J.M.; Brown, J.H.; Colwell, R.K.; Fuhrman, J.A.; Green, J.L.; Horner-Devine, M.C.; Kane, M.; Krumins, J.A.; Kuske, C.R.; et al. Microbial biogeography: Putting microorganisms on the map. *Nat. Rev. Microbiol.* **2006**, *4*, 102–112.
52. Vicuña, R.; González, B. The microbial world in a changing environment. *Rev. Chil. De Hist. Nat.* **2021**, *94*, 2.
53. Katiyar, V. Assessment of indoor air micro-flora in selected schools. *Adv. Environ. Res.* **2013**, *2*, 61–80.
54. Li, Y.; Lu, R.; Li, W.; Xie, Z.; Song, Y. Concentrations and size distributions of viable bioaerosols under various weather conditions in a typical semi-arid city of Northwest China. *J. Aerosol Sci.* **2017**, *106*, 83–92.
55. Lladó Fernández, S.; Větrovský, T.; Baldrian, P. The concept of operational taxonomic units revisited: Genomes of bacteria that are regarded as closely related are often highly dissimilar. *Folia Microbiol.* **2019**, *64*, 19–23.
56. He, Y.; Caporaso, J.G.; Jiang, X.-T.; Sheng, H.-F.; Huse, S.M.; Rideout, J.R.; Edgar, R.C.; Kopylova, E.; Walters, W.A.; Knight, R.; et al. Stability of operational taxonomic units: An important but neglected property for analyzing microbial diversity. *Microbiome* **2015**, *3*, 20.
57. Roswell, M.; Dushoff, J.; Winfree, R. A conceptual guide to measuring species diversity. *Oikos* **2021**, *130*, 321–338.
58. Wei, K.; Zheng, Y.; Li, J.; Shen, F.; Zou, Z.; Fan, H.; Li, X.; Wu, C.-Y.; Yao, M. Microbial aerosol characteristics in highly polluted and near-pristine environments featuring different climatic conditions. *Sci. Bull.* **2015**, *60*, 1439–1447.
59. Menut, L.; Siour, G.; Bessagnet, B.; Couvidat, F.; Journet, E.; Balkanski, Y.; Desboeufs, K. Modelling the mineralogical composition and solubility of mineral dust in the Mediterranean area with CHIMERE 2017r4. *Geosci. Model Dev.* **2020**, *13*, 2051–2071.
60. Cavender-Bares, J.; Schneider, F.D.; Santos, M.J.; Armstrong, A.; Carnaval, A.; Dahlin, K.M.; Fatoyinbo, L.; Hurtt, G.C.; Schimel, D.; Townsend, P.A.; et al. Integrating remote sensing with ecology and evolution to advance biodiversity conservation. *Nat. Ecol. Evol.* **2022**, *6*, 506–519.
61. Han, Y.; Li, L.; Wang, Y.; Ma, J.; Li, P.; Han, C.; Liu, J. Composition, dispersion, and health risks of bioaerosols in wastewater treatment plants: A review. *Front. Environ. Sci. Eng.* **2020**, *15*, 38.
62. Liu, Z.; Zhuang, W.; Hu, L.; Rong, R.; Li, J.; Ding, W.; Li, N. Experimental and numerical study of potential infection risks from exposure to bioaerosols in one BSL-3 laboratory. *Build. Environ.* **2020**, *179*, 106991.
63. Sheikhnejad, Y.; Aghamolaei, R.; Fallahpour, M.; Motamedi, H.; Moshfeghi, M.; Mirzaei, P.A.; Bordbar, H. Airborne and aerosol pathogen transmission modeling of respiratory events in buildings: An overview of computational fluid dynamics. *Sustain. Cities Soc.* **2022**, *79*, 103704.
64. Peng, S.; Chen, Q.; Liu, E. The role of computational fluid dynamics tools on investigation of pathogen transmission: Prevention and control. *Sci. Total Environ.* **2020**, *746*, 142090.
65. Fairs, A.; Agbetile, J.; Bourne, M.; Hargadon, B.; Monteiro, W.R.; Morley, J.P.; Edwards, R.E.; Wardlaw, A.J.; Pashley, C.H. Isolation of Aspergillus fumigatus from sputum is associated with elevated airborne levels in homes of patients with asthma. *Indoor Air* **2013**, *23*, 275–284.
66. Leleu, C.; Menotti, J.; Meneceur, P.; Choukri, F.; Sulahian, A.; Garin, Y.J.-F.; Denis, J.-B.; Derouin, F. Bayesian Development of a Dose-Response Model for Aspergillus fumigatus and Invasive Aspergillosis. *Risk Anal.* **2013**, *33*, 1441–1453.
67. Wang, M.; Kong, W.; Marten, R.; He, X.-C.; Chen, D.; Pfeifer, J.; Heitto, A.; Kontkanen, J.; Dada, L.; Kürten, A.; et al. Rapid growth of new atmospheric particles by nitric acid and ammonia condensation. *Nature* **2020**, *581*, 184–189.